Deformation Texture Analysis Based on Crystal Plasticity in Heavily Cold-Rolled 3% Si Steel

Noriki Fujita[1], Masanori Takenaka[2]

[1]JFE Steel Corporation, Steel Research Laboratory
1-1 Minamiwatarida-cho, Kawasaki, JAPAN, 210-0855
Phone: +81-44-322-6536
Email: no-fujita@jfe-steel.co.jp

[2]JFE Steel Corporation, Steel Research Laboratory
1 Mizushima Kawasakidori, Kurashiki, JAPAN, 712-8511
Phone: +81-86-447-3935
Email: m-takenaka@jfe-steel.co.jp

ABSTRACT

3% Si steel is a critical soft magnetic material widely used in the cores of motors and generators, significantly impacting the efficiency of these devices. Enhancing magnetic flux density and reducing energy loss (iron loss) are essential for energy conservation. To align the <001> easy magnetization axis of iron in the product's magnetization direction, it is necessary to control over the primary recrystallization texture, such as {111}<112>.

While the development mechanism of primary recrystallization texture is linked to the cold rolling reduction rate and has been extensively studied in automotive steel sheets, the origins of deformation and recrystallization texture development during heavy cold rolling remain unclear. Given the importance of nucleation orientation theory in recrystallization texture development, understanding the development mechanism of cold rolling texture, particularly {100}<011> texture, during heavy cold rolling is crucial.

This study applied crystal plasticity finite element model (CPFEM) to cold rolling to evaluate the development of cold rolling texture in heavily cold-rolled 3% Si steel. Crystal plasticity simulation implied that the combined effect of pencil-glide slips and twinning contributes significantly to the development of the {100}<011> cold-rolling texture in heavily cold-rolled 3% Si steel.

The findings contribute to a deeper understanding of texture development mechanisms, potentially leading to improved material properties and energy efficiency in industrial applications.

Keywords: cold rolling, silicon steel, texture evolution, crystal plasticity

INTRODUCTION

3% Si steel is widely used as a core material in motors and generators, and it is a crucial soft magnetic material that significantly influences the efficiency of these devices. From the perspective of energy conservation, it is essential to enhance the magnetic flux density and reduce energy losses (iron losses). Generally, to increase the magnetic flux density of the material, it is preferable to align the easy magnetization axis of iron, the <001> direction, with the magnetization direction of the product. To achieve this, it is important to control the primary recrystallization texture, such as {111}<112> [1].

The development mechanism of primary recrystallization texture is derived from the cold rolling reduction rate [2]. Due to the improvement in formability, such as the r-value, it has been extensively studied in the field of automotive steel sheets [3].

However, the origin of the development of deformation and recrystallization textures during severe cold rolling processing remains unclear. Quadir and Duggan investigated the recrystallization behavior of IF steel subjected to 95% cold rolling and demonstrated that recrystallization nuclei originate near the deformation bands formed within {100}<011> deformed grains

[4]. Additionally, Takenaka et al. showed that the primary recrystallization texture develops through the change of active slip systems in severe cold rolling to C-added 3% silicon steel [5].

Since the nucleation orientation theory has been suggested as a mechanism for the development of recrystallization texture, it is important to clarify the development mechanism of cold rolling texture, particularly the {100}<011> cold rolling texture formed by severe cold rolling processing. In recent years, crystal plasticity analysis has been actively conducted as a method to predict deformed texture. However, there are few examples of its application to the cold rolling process of 3% Si steel. In this study, the development of cold rolling texture in severely cold-rolled 3% Si steel was evaluated by crystal plasticity FEM.

CRYSTAL PLASTICITY MODELLING

Constitutive Model

Crystal plasticity analysis was performed to evaluate the influence of the plastic deformation behavior on the evolution of the cold-rolling texture under high rolling reductions, as shown in Fig.1. The crystal plasticity analysis was based on the assumption that plastic deformation proceeds along specific shear vectors on certain slip planes [6]. The DAMASK framework [7] was used for the crystal plasticity analysis, as shown in Fig.2.

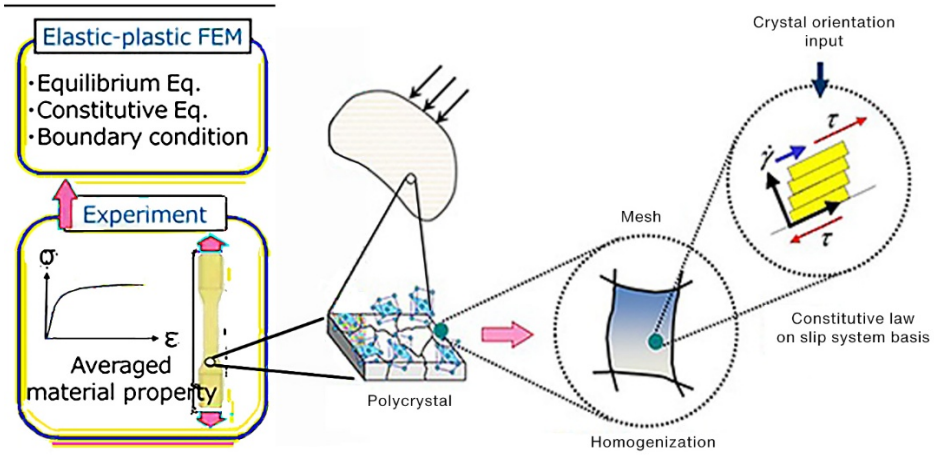

Figure 1. Crystal plasticity analysis.

In silicon steels, both deformation twins and slips are often observed [8, 9]. Therefore, it is necessary to consider the deformation twin evolution by crystal plasticity simulation. A probabilistic twin nucleation model [10], composite grain model [11] and predominant twin reorientation model [12] have been proposed for numerical description of deformation twins. In these models, crystal rotation and shear strain by the deformation twin are modelled separately. When a certain threshold is satisfied, crystal rotation of the deformation twin is applied.

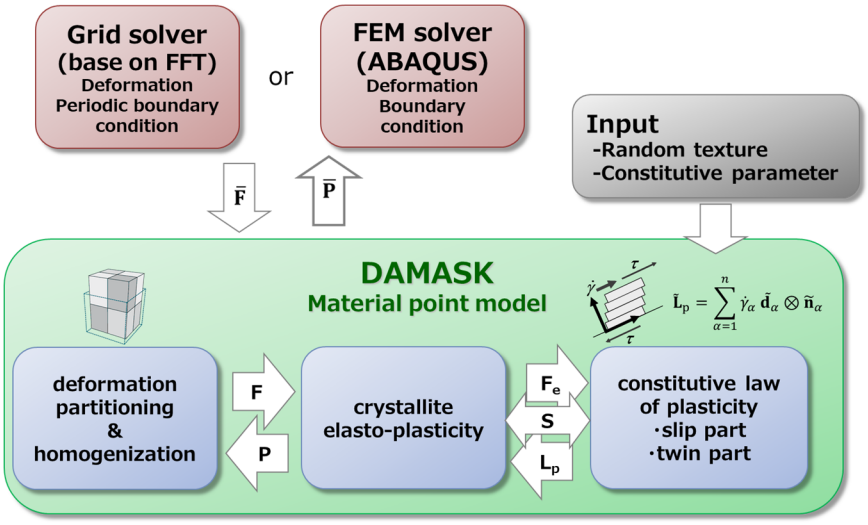

Figure 2. Crystal plasticity framework.

However, in analyses under high reductions, it is assumed that a large crystal rotation by the deformation twin causes an unstable result, such as excessive element distortion. Therefore, in this study, the incorporation model [13] was applied for the evolution of cold-rolling texture under a high reduction. The incorporation model allows slip deformation in the twin generation area. The plastic velocity gradient tensor $\mathbf{L}_p$, is given by the summation of plastic slip in each slip system or twin system, as shown in Eq. (1):

$$\mathbf{L}_p = (1 - \sum_{\beta=1}^{Ntwin} f^{\beta}) \sum_{\alpha=1}^{N_{slip}} \dot{\gamma}^{\alpha} S^{\alpha} + \sum_{\beta=1}^{Ntwin} f^{\beta} \dot{\gamma}^{\beta} S^{\beta} \quad (1)$$

where, N_{slip} and N_{twin} are the number of active slip and twin systems, respectively. A BCC crystal structure with

{110}<111> and {112}<111> slip system families was used. Raabe [14] reported that the contribution of {123} slip system families in crystal plasticity simulation is small. Similarly, the twin crystal structure with {112}<111> slip system families was used for the matrix. $\dot{\gamma}^{\alpha}$ and $\dot{\gamma}^{\beta}$ are the shear strain rates in slip and twin systems, respectively. S^{α} and S^{β} are the slip resistance in each slip and twin system, respectively (α=1, 2, …, 24; β=1, 2, …, 12). f^{β} is the twin volume fraction rate. The strain rate in each slip system is given by a rate dependent model, as shown in Eqs. (2)~(4). The hardening equation is given by Eq. (5).

$$S^{\alpha} = \sum_{i=1}^{24} \dot{\gamma}^{i} h^{\alpha} \left| 1 - \frac{S^{\alpha}}{S_{\infty}^{\alpha}} \right|^{w} \operatorname{sgn}\left(1 - \frac{S^{\alpha}}{S_{\infty}^{\alpha}}\right) \quad (2)$$

$$S_{\infty}^{\alpha} = S_{0\infty}^{\alpha} + S_{pr} \sqrt{\sum_{\beta} f^{\beta}} \quad (3)$$

$$h^{\alpha} = h_0 \left(1 + C\left(\sum f^{\beta}\right)^{B}\right) \quad (4)$$

$$\dot{\gamma}^{\alpha} = \dot{\gamma}_0 \left| \frac{\tau^{\alpha}}{S^{\alpha}} \right|^{n} \operatorname{sgn}(\tau^{\alpha}) \quad (5)$$

where $S_{0\infty}$ is the saturation slip resistance, h_0 is the initial hardening rate, w is the hardening exponent, n is the strain rate exponent, S_{pr} is the push-up factor for slip saturation due to twinning, B is an exponent to control the effect of the twin volume fraction on the hardening rate, C is the coefficient of the twin effect, $\dot{\gamma}_0$ is the reference shear strain rate and τ^{α} is the resolved shear stress on the slip system. The strain rate in each twin system is given by Eq. (6) and the twin volume fraction rate f^{β}, is given by Eq. (7).

$$S^{\beta} = h_0^{twin-twin} \left(\sum_{\beta} \gamma^{\beta}\right)^{D} \sum_{k} \gamma^{k} f^{k} + h_0^{twin-slip} \left(\sum_{\alpha} \gamma^{\alpha}\right)^{E} \sum_{k} \dot{\gamma}^{k} \quad (6)$$

$$f^{\beta} = \frac{\dot{\gamma}^{\beta}}{\gamma^{\beta}} \left| \frac{\tau^{\beta}}{S^{\beta}} \right|^{n} H(\tau^{\beta}) \quad (7)$$

where $h^{twin-twin}$ is the hardening rate with twin interaction, $h^{twin-slip}$ is the hardening rate with slip-twin interaction, D and E are fitting parameters, H is the Heaviside function and τ^{β} is the resolved shear stress on the twin system. Table 1 shows the material parameters used in the crystal plasticity simulation. Fig. 1 shows the strain-stress curves obtained from the tensile tests (black line) and crystal plasticity simulations (red line). The material properties used to describe the hardening behavior due to the slip and twin interactions were estimated from the macroscopic strain-stress curves taken from Fig. 3.

Table 1. Material parameters used in the crystal plasticity simulations.

	Description	3% Si steel	Unit
C_{11}	Elastic constant	233.3×10^3	MPa
C_{12}	Elastic constant	135.5×10^3	MPa
C_{44}	Elastic constant	118.0×10^3	MPa
$\dot{\gamma}_0$	Reference shear strain rate	1.0×10^{-3}	s^{-1}
$S_{[110]}$	Slip resistance in [110] slip system	220	MPa
$S_{0\infty[110]}$	Saturation slip resistance	255	MPa
$S_{[112]}$	Slip resistance in [112] slip system	240	MPa
$S_{0\infty[112]}$	Saturation slip resistance	300	MPa
$h_{0[110]}$	Initial hardening rate in [110] slip system	5000	MPa
$h_{0[112]}$	Initial hardening rate in [112] slip system	1000	MPa
n	Strain rate exponent	20	
w	Hardening exponent	1.00	
S_{pr}	Push-up factor for slip saturation due to twinning	200	MPa
B	Hardening exponent for twin effect	2	
C	Coefficient for twin effect	30	
D	Hardening parameter	2	
E	Hardening parameter	2	
S^{β}	Slip resistance in twin system	140	MPa
$h_0^{twin\text{-}twin}$	Hardening rate for twin	200	MPa
$h_0^{twin\text{-}slip}$	Hardening rate for twin-slip interaction contribution	200	MPa

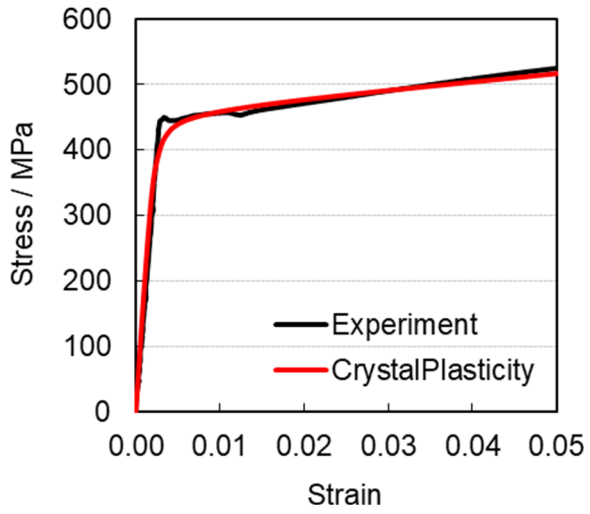

Figure 3. Comparison of the flow curves obtained from numerical prediction.

CONDITIONS OF COLD ROLLING SIMULATION

The cold-rolling process was simulated using a finite element method (FEM) code (ABAQUS Standard ver. 6.14) with the DAMASK user subroutine. The elements applied for the material were 3D isoparametric elements with reduced integration (C3D8R), and the total number of elements was 512 ($8 \times 8 \times 8$). After embedding the initial crystal orientation in each element, compression of 90% was applied under the plane strain condition at a strain rate of 1.0 s^{-1}. Embedded initial crystal orientations were generated from the measured ODFs (Orientation Distribution Functions) using the method by Morawiec et al. [15].

In the ODF, the orientation density for each specific angle represented by Bunge Euler angle ($\varphi_1, \Phi, \varphi_2$), is organized in the three-dimensional space, as shown in Fig.4. As shown in Fig. 5, information on the representative deformation texture can be obtained from the 45° section. The Euler angle was generated randomly using Eq. (8) and the intensity of the ODFs corresponding to the generated Euler angle was extracted. When the intensity of the ODFs satisfies Eq. (9), the crystal orientation is regenerated. In Eq. (9), f_{max} is the maximum intensity of the ODFs.

$$f(\varphi_1, \Phi, \varphi_2) = \sum_{l=0}^{\infty} \nabla_{m=-l}^{l} \sum_{n=-l}^{l} C_l^{mn} T_l^{mn}(\varphi_1, \Phi, \varphi_2) \tag{8}$$

$$\begin{aligned} \varphi_1 &= 180° \times rand(\ \ ) \\ \{\Phi &= cos^{-1}\{rand(\ \ )\}\} \\ \varphi_2 &= 90° \times rand(\ \ ) \end{aligned} \tag{9}$$

$$f(\varphi_1, \Phi, \varphi_2) \geq f_{max} \times rand(\ \ ) \tag{10}$$

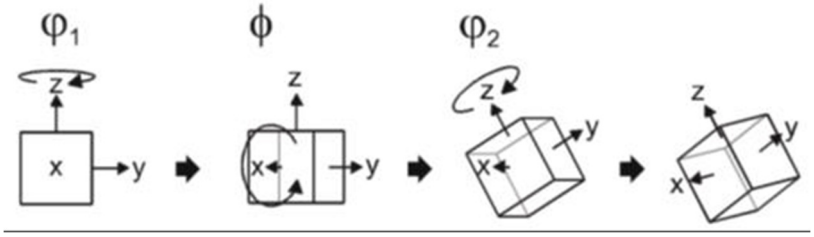

Figure 4. Bunge Euler angle.

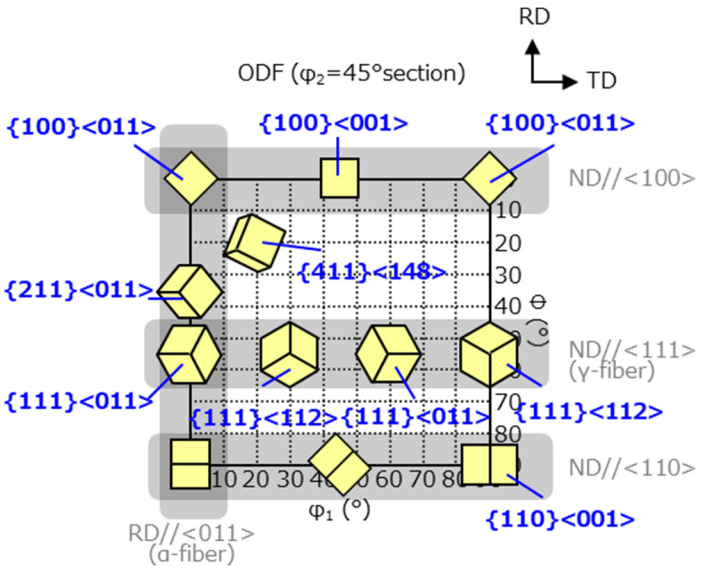

Figure 5. The $\varphi_2 = 45°$ cross section of ODF showing representative texture components of the BCC crystal.

SIMULATION RESULTS

The deformed texture was predicted using crystal orientation information after rolling by different reductions. Fig. 4 shows the deformed texture evolution obtained from the crystal plasticity simulation with various active slip/twin systems. The ODFs in the cross section of $\varphi_2 = 45°$ are shown as representative textures. Fig. 6(a)-(c) show the results for the {110}<111> slip system without twinning (N_{slip}=12, N_{twin}=0), the {110}<111> and {112}<111> slip systems without twinning (N_{slip}=24, N_{twin}=0) and the {110}<111> and {112}<111> slip systems with the {112}<111> twinning system (N_{slip}=24, N_{twin}=12), respectively.

When the BCC crystal structure with the {110}<111> slip system without twinning was simulated, high intensities of {111}<112> were predicted under a high rolling reduction of 90%. When the BCC crystal structure with the {110}<111> and {112}<111> slip systems without twinning was applied, high intensities of {111} <110> and higher intensities of α-fiber were predicted. In both cases, the intensities of {100}<011> were small. On the other hands, when the BCC crystal structure with the {110}<111> slip system and the {112}<111> twinning system was considered, a slightly higher intensity of {100}<011> than the crystal plasticity simulation without the twin system was predicted under a high rolling reduction of 90%.

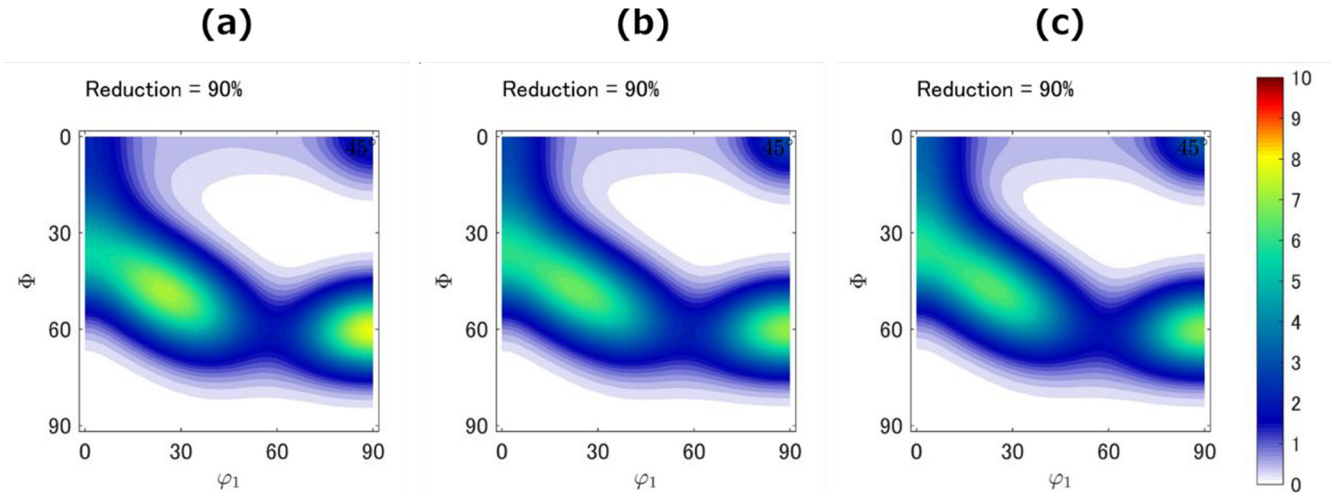

Figure 6. Cold-rolled texture evolution predicted by crystal plasticity simulation in 3% Si steel.

(φ_2=45-degree cross-section)
(a) 12 slip systems without twin systems,
(b) 24 slip systems without twin systems,
(c) 24 slip systems with twin systems

Fig. 7 shows the influence of various active slip/twin systems on the intensity of {100}<011>. As the rolling reduction rate increases, the intensity of {100}<011> also increases. However, the intensity of {100}<011> slightly increased when either pencil-glide slip deformation or twinning were considered. When both pencil-glide slips and twinning are considered, results in a higher intensity of {100}<011>. Therefore, it is considered that a combined effect through interaction between multiple slip systems and deformation twin would contribute significantly to the development of the cold-rolling texture with high intensities of {100}<011> experimentally observed in 3% Si steel.

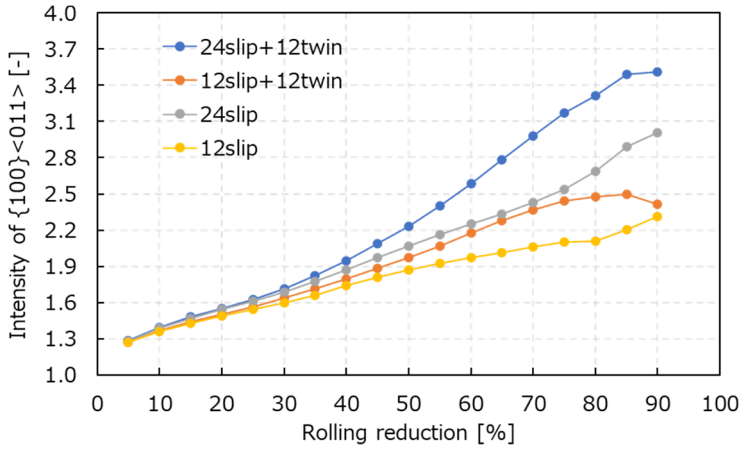

Figure 7. Influence of slip/twin systems on the intensity of {100}<011>.

CONCLUSIONS

The development of cold-rolling texture in heavily cold-rolled 3% Si steel was investigated theoretically. Based on crystal plasticity simulation, it is assumed that the combined effect of pencil-glide slip deformation and twinning has a significant contribution to the development of the {100}<011> cold-rolling texture in heavily cold-rolled 3% Si steel.

REFERENCES

1. T. Kumano, T. Haratani, Y. Ushigami, "The Improvement of Primary Texture for Sharp Goss Orientation on Grain Oriented Silicon Steel", *ISIJ Int.* 43, 2003, pp 736-745.
2. W.B. Hutchonson, "Development and control of annealing textures in low-carbon steels", *Int. Met. Rev.* 29, 1984, pp 25-42.
3. R.H. Heyer, D.E. McCabe, J.A. Elias, *Flat Rolled Products III*, Wiley, New York, Vol. 16, 1962, pp 29-46.
4. M.Z. Quadir, B.J. Duggan, "Deformation banding and recrystallization of α fibre components in heavily rolled IF steel", *Acta Mater.* 52, 2004, pp 4011-4021.
5. M. Takenaka et al., "Influence of carbon content on cold rolling and recrystallization texture in polycrystalline 3% Si- Fe", *IOP Conf. Ser. Mater. Sci. Eng.* 82, 2015, 012042.
6. F. Roters et al., "Overview of constitutive laws, kinematics, homogenization and multiscale methods in crystal plasticity finite-element modeling: Theory, experiments, applications", *Acta Mater.* 58, 2010, pp 1152-1211.
7. F. Roters et al., "DAMASK – The Düsseldorf Advanced Material Simulation Kit for modeling multi-physics crystal plasticity, thermal, and damage phenomena from the single crystal up to the component scale", *Comp Mater Sci.* 158, 2019, pp 420-478.
8. T. Mizuguchi, K. Ikeda, N. Karasawa, "Effects of Temperature and Strain Rate on Deformation Twinning in Fe-Si Alloy", *ISIJ Int.* 55, 2015, pp 1496-1501.
9. H. Fu, Z. Zhang, Y. Jiang, J. Xie, "Applying the grain orientation dependence of deformation twinning to improve the deformation properties of an Fe-6.5 wt%Si alloy", *J. Alloy. Comp.* 689, 2016, pp 307-312.
10. I.J. Beyerlein, R.J. McCabe, C.N. Tomé, "Effect of microstructure on the nucleation of deformation twins in polycrystalline high-purity magnesium: A multi-scale modeling study", *J. Mech. Phys. Solids* 59, 2011, pp 988-1003.

11. G. Proust, C.N. Tomé, G.C. Kaschner, “Modeling texture, twinning and hardening evolution during deformation of hexagonal materials”, *Acta Mater.* 55, 2007, pp 2137-2148.
12. C.N. Tomé, R.A. Lebensohn, U.F. Kochs, “C.N. Tome, R.A. Lebensohn, U.F. Kocks, A model for texture development dominated by deformation twinning: Application to zirconium alloys, Acta”, *Acta Metall.* 39, 1991, pp 2667-2680.
13. S.R. Kalidindi, “Incorporation of deformation twinning in crystal plasticity models”, *J. Mech. Phys. Solids* 46, 1998, pp 267-290.
14. D. Raabe, “Investigation of contribution of {123} slip planes to development of rolling textures in bee metals by use of Taylor models”, *Mater. Sci. Technol.* 11, 1995, pp 455-460.
15. A. Morawiec, J.A. Szpunar, D.C. Hinz, “Texture influence on the frequency of occurrence of CSL-boundaries in polycrystalline materials”, *Acta Metall.* 41, 1993, pp 2825-2832.

